INVESTIGATION OF THE HEXACHIRAL HONEYCOMB EMC PROPERTIES BY FULL WAVE ELECTROMAGNETIC SIMULATION

Romeo-Cristian Ciobanu
Cristina Schreiner
Dept. of Electrical Measurements and Materials
Technical University Iasi, Romania
Iasi, 700050, Romania
E-mail: rciobanu@ee.tuiasi.ro

Radu-Florin Damian
Dept. of Telecommunications
Technical University Iasi, Romania
Iasi, 700506, Romania
E-mail: rdamian@etc.tuiasi.ro

KEYWORDS

Hexachiral honeycomb, Full wave electromagnetic, CST Microwave Studio

ABSTRACT

A hexachiral honeycomb structure with good mechanical properties, is investigated through full wave electromagnetic simulation. This new material shows some interesting EMC properties and promises better performance using different insertion techniques. The effect of the electromagnetic chirality is investigated. Design maps and thermal computations are derived.

I. INTRODUCTION

In the past years, an increasing amount of effort has been invested in the development of new materials, with good mechanical properties, low weight and low cost. In particular auxetic materials benefit from their negative Poisson's ratio (Grima 2007) and are investigated closely in the last decade (Li et al. 2000, Ammari et al. 1998, Oussaid R. and Haraoubia B. 2004). In the same time, we witness an increased utilization of the RF spectrum, especially in the free bands (2.4GHz). Coding techniques have been developed to ensure the "peaceful" coexistence of multiple emitter/receiver pairs in the same frequency band. In some cases, these techniques are not sufficient, especially when good shielding for an enclosure is imperative (aeronautics - Bornengo D. et al. 2005, medicine etc.). A natural step forward is to investigate the electromagnetic properties of these materials, in order to provide good electromagnetic shielding.

Electromagnetic metamaterials are defined as artificial effectively homogeneous electromagnetic structures with unusual properties not readily available in nature. An effectively homogeneous structure is a structure whose structural average cell size L is much smaller than the guided wavelength λ_g. i.e. the average cell size should be at least smaller than a quarter of wavelength (Caloz and Itoh 2006),

$$L < \frac{\lambda_g}{4} \tag{1}$$

The condition (1) is known as the effective-homogeneity limit or effective-homogeneity condition, and ensures that refractive phenomena will dominate over scattering/diffraction phenomena when a wave propagates inside the medium. In the present application, the frequency range of interest (1 to 15GHz) implies a guided waveguide between 10 mm and 150 mm, and we expect the chirality defined by geometry to play an electromagnetic role, depending on the cell size, especially at higher frequencies (7 to 15 GHz).

Depending on the method used for defining the magnetoelectric dyadics, there are multiple constitutive relations in extensive use for chiral mediums: Drude-Born-Fedorov (Athanasiadis and Costakis 2000, Oksanen et al. 1992) Post (Jaggard et al. 1988), Tellegen (Qiu et al. 2007). Equivalence between these relations can be obtained (Liu and Li 1999) by substitution in Maxwell's equations.

Widely used are Post constitutive relations in the frequency domain, valid for time harmonic electromagnetic fields: Eqs. (2), (3).

$$\mathbf{D} = \varepsilon_c \mathbf{E} + j\xi_c \mathbf{B} \tag{2}$$

$$\mathbf{H} = j\xi_c \mathbf{E} + \mathbf{B}/\mu_c \tag{3}$$

where ε_c and μ_c represent an equivalent of the permittivity and permeability, ξ_c the chirality admittance, which is a measure of the handedness of the medium and j is the imaginary unit.

II. SIMULATION SETUP

The structure used in tests was a fiber reinforced polymer prototype, developed in the framework of the CHISMACOMB (CHIral SMArt honeyCOMB) FP6-EU-013641 project (Chismacomb 2008), by Italcompany (figure 1). The structure is a hexachiral honeycomb, each of the equally spaced cylinders being connected to his 6 neighbors by ligaments and is based on the idea found in (Prall and Lakes 1997) which is a simplification of a two-dimensional molecular model studied earlier (Wojciechowski 1989).

Proceedings 23rd European Conference on Modelling and Simulation ©ECMS Javier Otamendi, Andrzej Bargiela, José Luis Montes, Luis Miguel Doncel Pedrera (Editors)
ISBN: 978-0-9553018-8-9 / ISBN: 978-0-9553018-9-6 (CD)

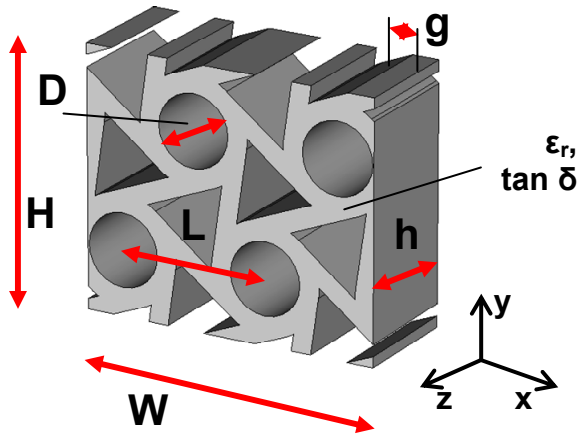

Figure 1: Rectangular Unit Cell.

The interaction between a plane wave and an infinitely large sheet of auxetic material at normal incidence was investigated. The boundary conditions were set to electric wall (both walls on x directions) and magnetic wall (y direction walls). An input wave port was placed at a distance equal to the minimum between the 8th part of the wavelength and 5 mesh lines from the structure, the second (exit) wave port is added only when losses inside the structure were taken into account.

In order to limit the model's dimensions, the periodicity of the structure was investigated. While the intrinsic unit cell for this structure will contain only one cylinder and half of every surrounding ligament, numerical electromagnetic computation demands a rectangular unit cell which can be placed on a regular (not staggered) rectangular grid in order to preserve electromagnetic fields symmetries. The rectangular unit cell is showed in figure 2, the length and width being equal to $W = 2 \cdot L$ (x direction) and $H = L \cdot \sqrt{3}$ (y direction) respectively (where L is the cylinder separation). Table 1 shows the typical dimensions used in tests when we parameterize the others.

Table 1: Typical Dimensions.

Parameter	Description	Value
D	Internal cylinder diameter	18.58 mm
L	Cylinder separation	24.72 mm
h	Height of the panel	19.75 mm
g	Ligament width	3.3 mm
ε_r	Electrical permittivity	2.5 (4)
tan δ	Loss angle tangent	0 (0.1-0.5)

The results of the simulations show the S parameters for the structure. The typical shielding parameters reflectance, transmittance and absorption are related to the S parameters by the following equations (Hong et al. 2003), as long as the surrounding medium is lossless:

$$R = |S_{11}|^2 \quad (4)$$

$$T = |S_{21}|^2 \quad (5)$$

$$A = 1 - R - T = 1 - |S_{11}|^2 - |S_{21}|^2 \quad (6)$$

III. ACCURACY OF THE RESULTS

The CST Microwave Studio frequency domain solver solves the problem for a single frequency at a time, and for a number of adaptively chosen frequency samples in the course of a frequency sweep. For each frequency sample, the linear equation system will be solved by an iterative (e.g. conjugate gradient) or sparse direct solver.

The CST Microwave Studio time domain solver calculates the development of fields through time at discrete locations and at discrete time samples. It calculates the transmission of energy between various ports and/or open space of the investigated structure.

For the hexachiral structure under test, the auxetic layer is illuminated with a plane wave, coming from the z direction, with normal incidence to the material. The polarization of the plane wave in the material is imposed by the electric/magnetic wall boundary conditions, and for correct calculations we expect the electromagnetic fields inside the structure to follow the characteristics of the incident wave. As in figure 2, we find that inside the hexachiral honeycomb, the electric field will have only E_x component, whereas the magnetic field shows only H_y component.

The final test was the comparison between the FDTD and FDFD analysis results for the same structure. The two computation methods are not related, even the mesh is different in this case (hexahedral with Perfect Boundary Approximation® - PBA for FDTD and tetrahedral for the frequency domain solver). The results are found to be essentially the same (see figure 3).

The difference between the two curves is maximum ±1dB in the 1÷10GHz range, except the frequencies around the reflection annulment, where a slight variation of the zero's frequency is detected (0.1GHz, meaning a 1.8% difference between the two minima) around 5.8GHz. The two solvers are independent even if they belong to the same software suite, so we can estimate a ±2dB general error coupled with a ±2% peak detection error for the rest of the simulations.

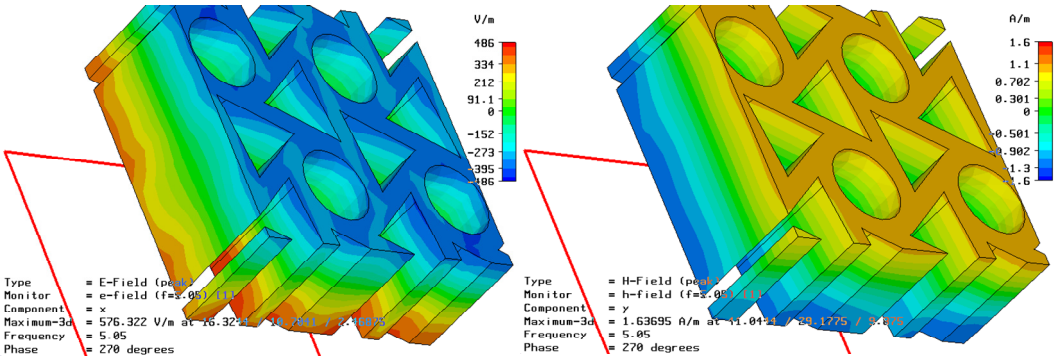

Figure 2: E_x (left) and H_y (right) Inside the Structure

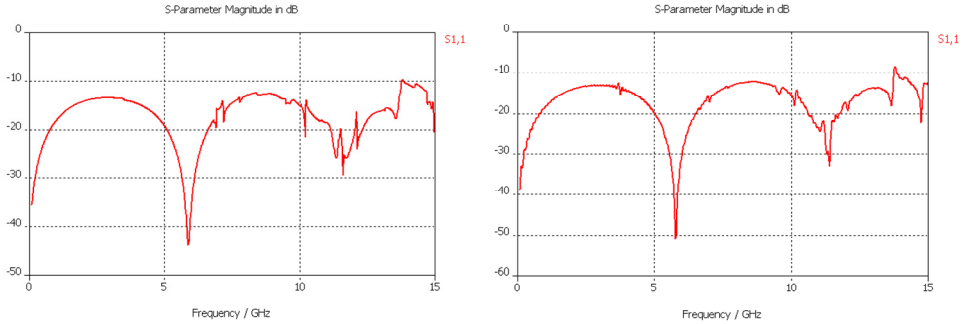

Figure 3: S_{11} for the Loseless Structure by FDFD (left) and FDTD (right) Computation

IV. RESULTS AND INFLUENCE OF CHIRALITY

Parametric studies investigated the effect of the dimensions (L, D, h, g) and material properties (ε, σ, tan δ). Figure 4 shows the influence of L, h (in this order) for the lossless dielectric over the reflection coefficient (S_{11}), and figure 5 shows the influence of ε and tan δ over reflection coefficient (S_{11}) or over the transmission coefficient (S_{21}) when losses are taken into account

Analysis shows that the chiral structure has almost identical properties (figures 4, 5) with an equivalent homogenous dielectric layer, so the mechanical and thermal advantages provided by the structure do not affect the electromagnetic properties in the bandwidth considered (0.1-10 GHz).

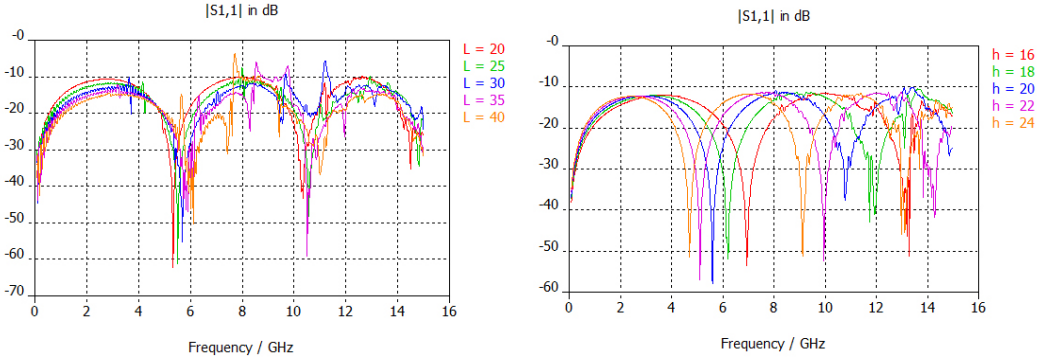

Figure 4: Cylinder Separation (L - left) and Layers' Height (h - right) Influence over S_{11}

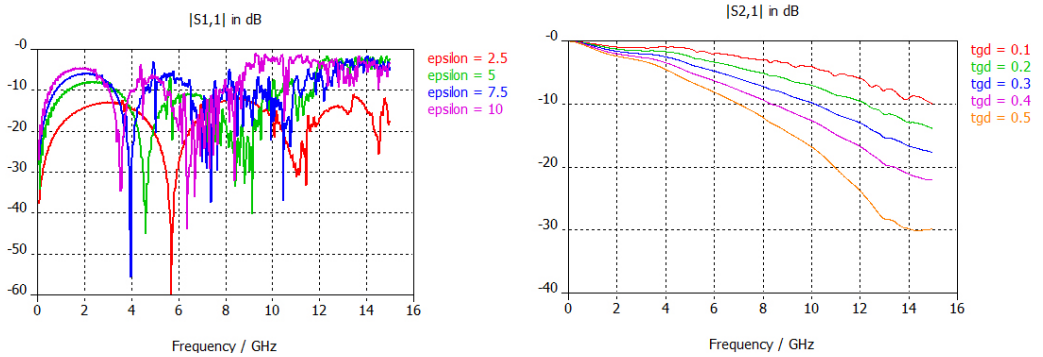

Figure 5: Electrical permittivity (ε - left) and Loss tangent (tan δ - right) influence over S_{11}/S_{22}

Figures 4-5 show that for the lossless chiral layer we have a typical half-wave reflectionless slab (Orfanidis 2008). We obtain zeroes for the reflection coefficient at the frequencies that verify the condition:

$$h = k \cdot \frac{\lambda_g}{2} = \frac{k}{2} \cdot \frac{c}{f\sqrt{\varepsilon_{eff}}} \tag{7}$$

where k must be an integer and λ_g is the guided wavelength, inside the equivalent homogenous dielectric slab. This behavior offers interesting electromagnetic applications, as radar invisibility or building wall transparency.

Equation (7) offers the possibility to use the results in figure 4 to investigate the variation of the effective electrical permittivity on the frequency. Every value for layer's height (h) generate at least two minima of the reflectivity in the bandwidth considered, corresponding to k=1, k=2 in equation (7). We can compute the effective electrical permittivity with equation (8).

$$\varepsilon_{eff}\left(f_{\min,k}\right) = \left(\frac{k \cdot c}{2 f_{\min,k} \cdot h}\right)^2 \tag{8}$$

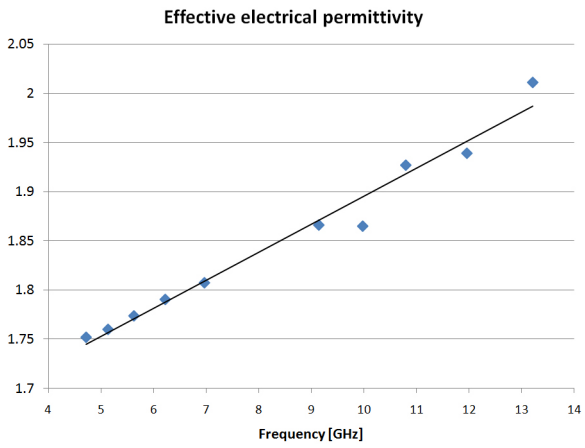

Figure 6. Effective electrical permittivity

The effective electrical permittivity increases linearly with the frequency, as the electromagnetic field is confined inside the dielectric at higher frequency. The results in figure 4 on which figure 6 is based are obtained for ε = 2.5 for the base material. In this case, we find the effective permittivity ranging from 1.61 to 2.1, depending on the frequency. In addition, as the frequency increases we notice slight variations from the predicted linear increase, as the chirality of the structure becomes more and more evident.

The effects of the chirality appear as we increase the frequency, the electrical permittivity and the cylinder separation. In the typical situation (table 1), equation (1) gives a frequency limit of about 2.37 GHz. Close inspection of the results (figure 4) shows that obvious effects of the microscopic chiral structure are visible at 8 GHz.

Condition (1) can be expressed in terms of visible influence as:

$$L \cdot f \cdot \sqrt{\varepsilon_{eff}} \approx \frac{3c}{4} \tag{9}$$

The other results verify this relationship. Increase of ε from 2.5 to 10 (figure 5) lower the frequency of appearance of chiral effects from 8GHz to 4 GHz (the square root of the permittivity factor of 4). Increase of L to 40 mm (figure 4) show the same effect starting from 5GHz.

We can conclude that regarding the hexachiral honeycomb, chirality influence becomes obvious when relation (9) applies, but while visible, this influence does not affect the macroscopic behavior of the panel under test. The hexachiral panel behaves as a homogenous dielectric, with a different effective electrical permittivity (figure 6).

V. PARAMETRIC ANALYSIS AND DESIGN MAPS

The results in figures 4, 5 offer important information regarding the behavior of the intrinsic chiral panel but are less suggestive from a macroscopic or "application" point of view. The macroscopic values of interest for a microwave shield designer are generally related to transmittance (figure 5b) at some critical frequencies (typically 0.9÷1GHz - the GSM band, 2.4 GHz - free use frequency bandwidth, and 5.8 GHz – a second free bandwidth) or reflectivity parameters (figures. 4-5a) as the frequency of the first minimum, the out of band maximum reflectivity (first and second maximum), depending on the application.

The question a designer is asked is rather an "inverse" of the answer from figures 4, 5. Usually the designer is not interested by the performance of "that" material, but instead the question is: "what material must I choose to obtain a certain transmittance or a certain reflectivity".
In the next set of analyses, the aim is to investigate the influence of the material properties (tan δ and ε) over the transmission and reflectivity properties.

Table 2: Geometric Parameters Sweep.

Parameter	Range	Step
D	20÷50 mm	5 mm
H	20÷50 mm	5 mm
L/D	1.5÷3	0.25
D/g	5÷20	2.5

In the first set of computations we maintain the same geometrical properties (D, L, h, g - Table 1) but we insert variations in material properties: tan δ = [0 , 0.5] and ε = [1.5 , 10]. S_{11} and S_{21} are computed. The parametric curves are plotted in figure 7 in order to facilitate shielding design with the hexachiral honeycomb. We represent the transmittance at the three

selected frequencies and the minima/maxima of the reflectance.

For the second set of computations we choose L/D and D/g ratios as important for the aspect ratio of the panel and with fixed dielectric parameters ($\varepsilon = 4$ and $\tan\delta = 0.01$) we make the transmission and reflection computation for geometric parameters as in Table 2. The results are plotted in figure 8.

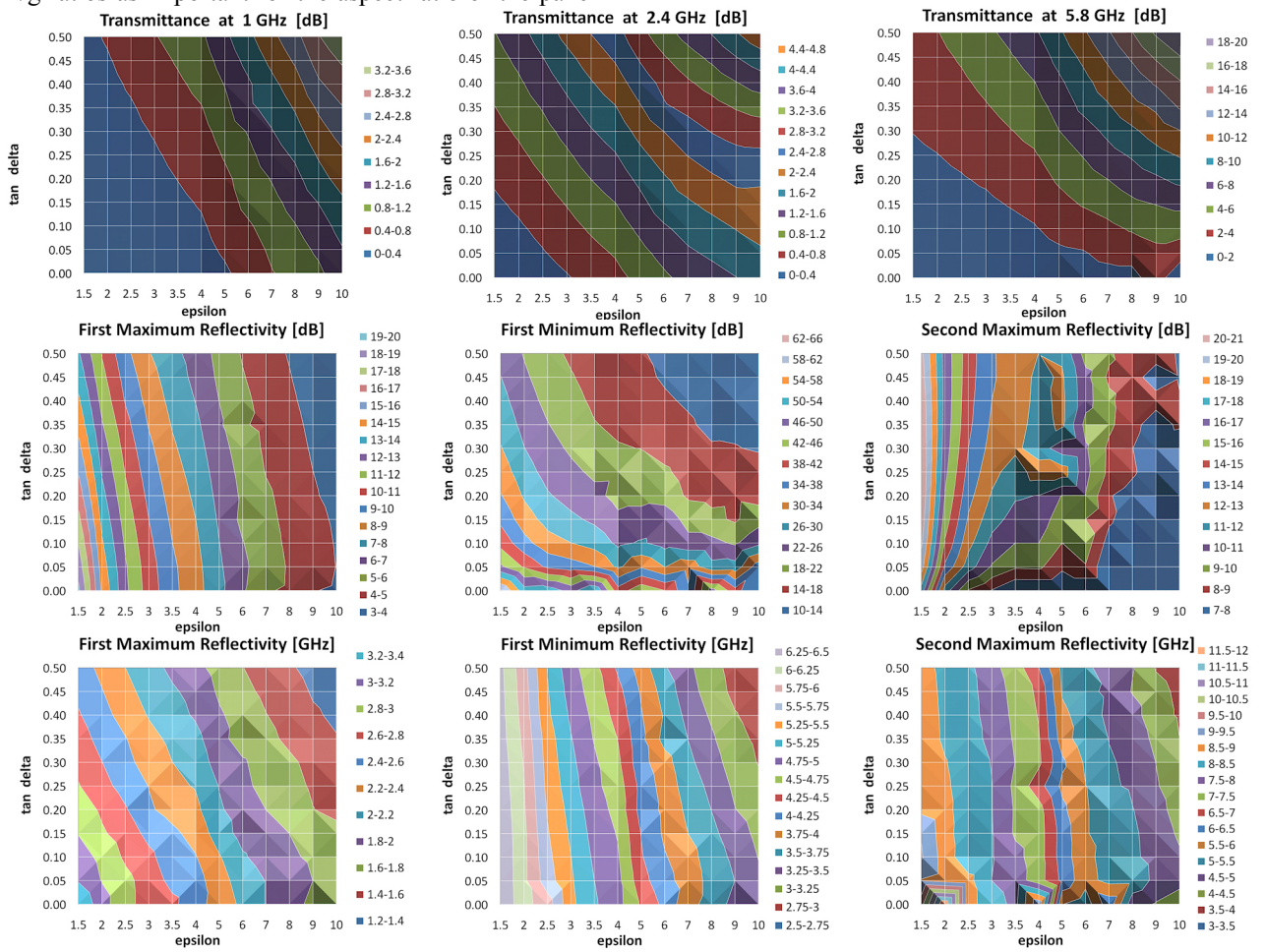

Figure 7 Dielectric Properties Design Maps.

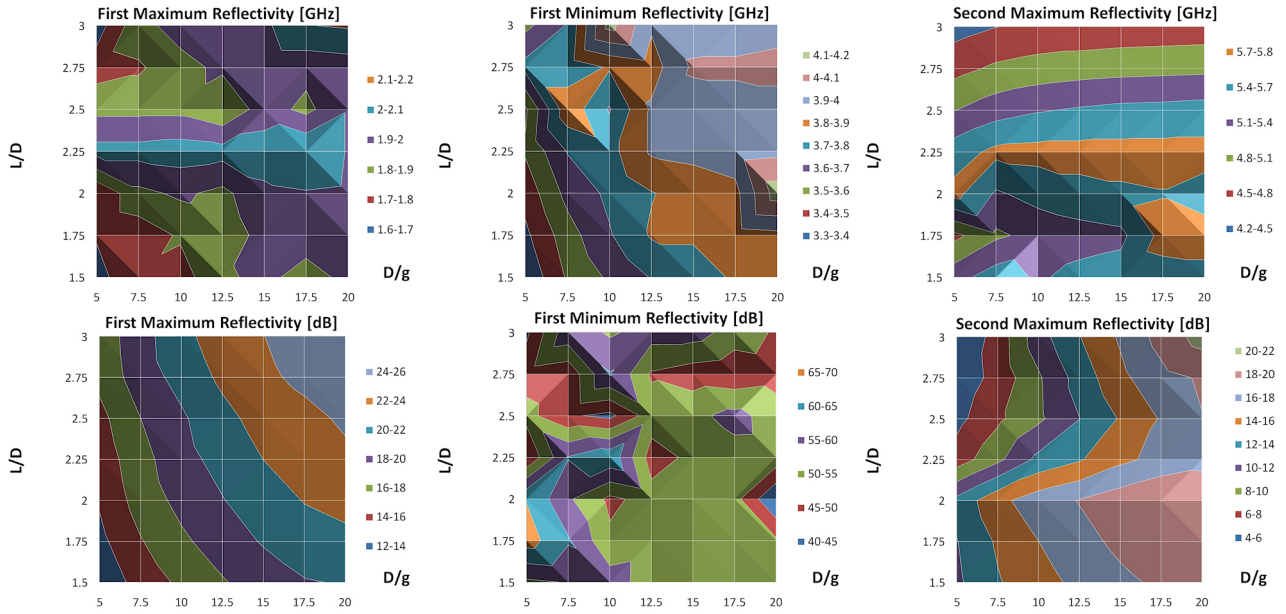

Figure 8 Geometric Properties Design Maps.

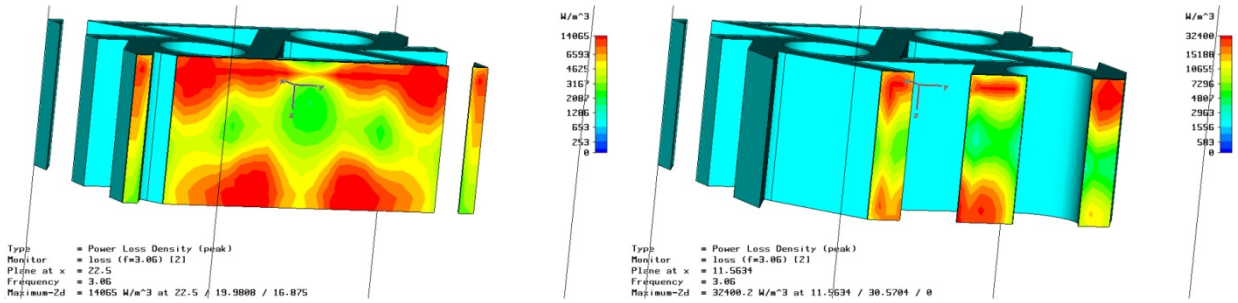

Figure 9: Power Loss Density at 3.06GHz

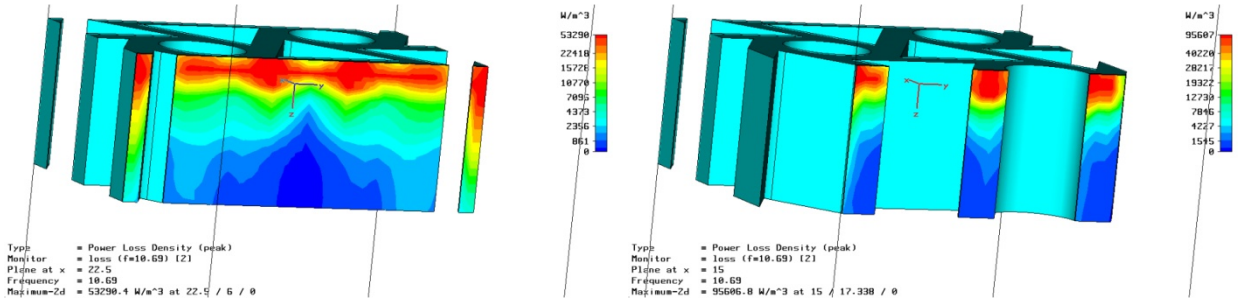

Figure 10: Power Loss Density at 10.69GHz

VI. THERMAL DISTRIBUTION

Simulations have been performed in order to identify the energy absorption characteristics inside the material. The first results emphasize an energy concentration depending solely on the hexachiral geometry. The power loss density inside the ligaments of the hexachiral honeycomb is an indication of energy dissipation inside the structure. The two frequencies chosen, 3.06GHz and 10.69GHz are those corresponding to a minimum of the reflectance (figure 9) and transmittance (figure 10) respectively, as the frequencies at which maximum thermal effect is expected.

A concentration of the energy dissipation will generate a temperature increase in certain points. However, this energy is not accumulated, the most significant heat transfer mechanism being thermal conduction (eq. 7). The speed of the heat transfer through a portion of material of transversal area A and length x depends on the steady state temperature difference.

Heat is generated differently in two points according to the electromagnetic energy concentration pattern (eq. 5). We can estimate the steady state for the thermal phenomenon when the difference between the generated heat in every point equals the heat transferred by conduction between the same points (eqs. 10-11).

$$\Delta\left(\frac{dQ}{dt}\right) = \left.\frac{dQ}{dt}\right|_1 - \left.\frac{dQ}{dt}\right|_2 = \Delta P_V \cdot dV \qquad (10)$$

$$\left.\frac{dQ}{dt}\right|_{1-2} = k \cdot A \cdot \frac{\Delta T}{x} \qquad (11)$$

We used the same software suite (CST Microwave Studio) described in section IV, with the difference that in single frequency analysis the FDFD (Finite Differences in Frequency Domain) solver was used to compute the fields inside the structure. The computation is full 3D, figures 9-10 show the power loss density in different longitudinal sections through the panel.

The power loss distribution is mainly longitudinal (in the direction of the incident wave). The incident illumination is 320W/m^2 (normalization: 1W over the surface of the input port), a rather high value if we consider that the safety limit for RF workers is 50W/m^2. While such a situation is not usually encountered, we can use eqs. (10), (11) to estimate the temperature gradient which will appear inside the hexachiral structure. At 3.06 GHz (figure 9), we have maximum $\Delta P_V \approx$ 12,000 W/m^3 and $\Delta P_V \approx$ 30,000 W/m^3 inside the cylinder and inside the ligaments respectively. The maximum temperature variation is $\Delta T \approx 4$ K and $\Delta T \approx$ 10 K respectively. As the power losses are related to transmission behavior, we expect greater effect when the transmittance reaches a minimum. At 10.69 GHz (figure 10), we have maximum $\Delta P_V \approx$ 53,000 W/m^3 and $\Delta P_V \approx$ 95,000 W/m^3 inside the cylinder and inside the ligaments respectively, the corresponding temperature variation being $\Delta T \approx 18$ K and $\Delta T \approx 33$ K respectively.

In typical applications (10 to 50 W/m^2 - safety limits) the effect is less important (up to 5K temperature differences) but the differences in temperature can reach 100K at 1kW/m^2 illumination. Wireless Power Transmission can use up to 30 ÷ 90 kW/m^2 at the space reflectors.

The simple hexachiral panel, subject to localized electromagnetic power dissipation develops thermal gradients which affect the mechanical performance thus thermal analysis in high power applications must rely on temperature gradient instead of uniformity.

CONCLUSIONS

In this paper a complete investigation of the hexachiral honeycomb by full wave electromagnetic simulation is performed. The software suite CST Microwave Studio is used, with the added benefit of the presence of multiple solvers. This allowed us to perform accuracy estimation (secton III) and extended the range of simulations we were able to perform.

The time domain solver (FDTD) was used in those situations where multiple simulations were needed and speed was an important issue (more than 10,000 different individual simulations were performed). Multiple parametric simulations were made, which allowed the investigation of the chirality in section IV and the derivation of the design maps in section V.

The frequency domain solver (FDFD) which is slower but more accurate in small bandwidths was used in order to verify the boundary conditions used (section II) and in order to investigate the microwave power distribution inside the material, which allowed the thermal analysis in section VI.

REFERENCES

Ammari H.; Laouadi M.; Nedelec J.-C.; 1998, "Low frequency behavior of solutions to electromagnetic scattering problems in chiral media", SIAM Journal. of Applied. Math, Society for Industrial and Applied Mathematics, Vol. 58, No. 3, 1022-1042, 1998

Athanasiadis C., Costakis G. 2000. "Electromagnetic scattering by a homogenous chiral obstacle in a chiral environement", IMA Journal of Applied Mathematics, Vol. 64 (2000), 245 - 258

Bornengo D.; Scarpa F.; Remillat C. 2005. "Evaluation of hexagonal chiral structure for morphing airfoil concept", Proceedings. IMechE Vol. 219 Part G: J. Aerospace Engineering, 185-192, 2005

Caloz C.; Itoh T.. 2006 "Electromagnetic metamaterials : transmission line theory and microwave applications: the engineering approach", John Wiley & Sons, Inc., Hoboken, New Jersey, 2006

Chismacomb 2008. "CHISMACOMB", FP6 Specific Target Research Project, FP6-EU-013641, http://www.chismacomb.eu/

Grima, J. 2007, "Negative, negative and more negative: systems exhibiting negative Poisson's ratio, negative thermal expansion and/or negative compressibility", 4th International Workshop on Auxetics and Related Systems, Malta, 2007, 8

Hong Y.K.; Lee C.Y.; Jeong C.K.; Lee D.E.; Kim K., Joo J. 2003 "Method and apparatus to measure electromagnetic interference shielding efficiency and its shielding characteristics in broadband frequency ranges", Review of Scientific Instruments, Volume 74, Issue 2, February 2003, 1098-1102

Jaggard D.L.; Sun X.; Engheta N. 1988. "Canonical Sources and Duality in Chiral Media", IEEE Transactions On Antennas And Propagation, Vol. 36, No. 7, July 1988, 1007-1013

Li, L.W.; You D.; Leong M.S. and Yeo T.S. 2000, "Electromagnetic scattering by multilayered chiral-media structures: a scattering-to-radiation transform , Journal of Electromagnetic Waves and Applications", Vol. 14, 401-404, 2000

Liu S.; Li L.W. 1999. "Mook-Seng Leong,Tat-Soon Yeo; "On the constitutive relations of chiral media and green's dyadics for an unbounded chiral medium", Microwave And Optical Technology Letters , Vol. 23, No. 6, 1999, 357 - 361

Oksanen M.; Koivisto P.; Tretyakov S. 1992. Vector Circuit Method Applied for Chiral Slab Waveguides, Journal Of Lightwave Technology, Vol. 10, No. 2, February 1992, 150-155

Orfanidis S.J. 2008. "Electromagnetic Waves and Antennas", Rutgers University online book, ch 5, 160-166, http://www.ece.rutgers.edu/~orfanidi/ewa/

Oussaid R.; Haraoubia B. 2004, "Behavior of a chiral material in terms of a guided wave propagation", International Journal of Applied Electromagnetics and Mechanics, vol. 19 , 2004, 631-635

Prall D; Lakes RS. 1997. "Properties of a chiral honeycomb with a poisson's ratio of - 1", Int. J. Mech. Sci. Vol. 39, No. 3, 305-314, 1997

Qiu C.W.; Yao H.Y.; Burokur S.N.; Zouhdi S., Li L.W. 2007. ."Electromagnetic Scattering Properties in a Multilayered Metamaterial Cylinder", IEICE Trans. Commun., Vol.E90–B, No.9 September 2007, 2423-2429

Wojciechowski K.W. 1989, "Two-dimensional isotropic systems with a negative Poisson ratio", Physics Letters A137, 60-64 (1989)